Rapid Alignment of Velocity and Magnetic Field in Magnetohydrodynamic Turbulence

W. H. Matthaeus,[1] A. Pouquet,[2] P. D. Mininni,[2,3] P. Dmitruk,[1,3] and B. Breech[1]

[1]*Bartol Research Institute and Department of Physics and Astronomy, University of Delaware, Newark, Delaware 18716, USA*
[2]*NCAR, P.O. Box 3000, Boulder, Colorado 80307-3000, USA*
[3]*Departamento de Física, Facultad de Ciencias Exactas y Naturales, Universidad de Buenos Aires, Ciudad Universitaria, 1428 Buenos Aires, Argentina*

(Received 3 August 2007; published 27 February 2008)

We show that local directional alignment of the velocity and magnetic field fluctuations occurs rapidly in magnetohydrodynamics for a variety of parameters and is seen both in direct numerical simulations and in solar wind data. The phenomenon is due to an alignment between magnetic field and gradients of either pressure or kinetic energy, and is similar to alignment of velocity and vorticity in Navier-Stokes turbulence. This rapid and robust relaxation process leads to a local weakening of nonlinear terms.

DOI: 10.1103/PhysRevLett.100.085003 PACS numbers: 52.35.Ra, 47.27.E−, 52.30.Cv, 96.50.Tf

In magnetohydrodynamic (MHD) turbulence, the fluctuations of magnetic field **b** and velocity **v** enter on nearly equal footing. One consequence is that the nonlinear MHD equations are linearized when **b** (in Alfvén speed units) is everywhere equal (or opposite) to **v**. Such "Alfvénic" states have a large cross-helicity (see below), or correlation between **v** and **b**, and have long been thought to be favored in relaxation processes [1], and are observed in the inner solar wind [2,3]. Global evolution towards Alfvénic states, or "dynamic alignment" [4], requires many nonlinear eddy turnover times. Here we describe a related, rapid relaxation process, in which local, directional near alignment of **v** and **b** emerges in less than one turnover time, for a variety of turbulence parameters. This process need not be associated with global alignment, but rather occurs independently in localized patches.

Dynamic alignment competes with other MHD relaxation processes [5], and, for some parameters, it does not occur or is incomplete. Solar wind observations show that the magnitude of the correlation between **v** and **b**, often called "Alfvénicity," decreases at larger heliocentric distance [3], in apparent contradiction to the dynamic alignment principle. There are suggestions that directional alignment (a necessary condition for global dynamic alignment) may be more ubiquitous. MHD relaxation can be described by a variational principle [5] in which cross-helicity and a magnetic invariant [helicity in three dimensions (3D), or mean square flux function in two dimensions (2D)] are held constant, while energy is minimized. The emergent Euler-Lagrange equations predict final states, in both 2D and 3D, and for all parameters, in which **v** and **b** are directionally aligned or antialigned. This theory is well confirmed by numerical simulations [5]. These ideas have been extended to explain steady state MHD spectral properties [6]. Evidently, in the long time limit, pointwise directional alignment is obtained more easily than is the global Alfvénic state. Here we show using numerical experiments that local directional alignment is even more robust and occurs rapidly as well as in local patches. We also show that alignment in the solar wind is consistent with this picture. This rapid relaxation can be understood by examination of the MHD equations. These features have not been fully recognized previously, and are analogous to the local emergence of Beltrami flows [7] in hydrodynamics.

MHD and Alfvénic states.—In familiar dimensionless Alfvén speed units, the equations of incompressible MHD are

$$\frac{\partial \mathbf{v}}{\partial t} + \mathbf{v}\cdot\boldsymbol{\nabla}\mathbf{v} = -\boldsymbol{\nabla}\mathcal{P} + \mathbf{j}\times\mathbf{b} + \nu\boldsymbol{\nabla}^2\mathbf{v}, \tag{1}$$

$$\frac{\partial \mathbf{b}}{\partial t} + \mathbf{v}\cdot\boldsymbol{\nabla}\mathbf{b} = \mathbf{b}\cdot\boldsymbol{\nabla}\mathbf{v} + \eta\boldsymbol{\nabla}^2\mathbf{b}, \tag{2}$$

with $\boldsymbol{\nabla}\cdot\mathbf{v} = \boldsymbol{\nabla}\cdot\mathbf{b} = 0$. Here, $\mathbf{b} = \boldsymbol{\nabla}\times\mathbf{a}$ with **a** the magnetic potential, the electric current density is $\mathbf{j} = \boldsymbol{\nabla}\times\mathbf{b}$, and $\mathcal{P}$ is the pressure. The viscosity ν and resistivity η define mechanical and magnetic Reynolds numbers, respectively, as $R_V = LU/\nu$ and $R_M = LU/\eta$, with spatial average $\langle\ldots\rangle$, $U = \langle|\mathbf{v}|^2\rangle^{1/2}$, and L a length (integral scale) associated with the large-scale flow. The energy $E = E_v + E_b = \langle|\mathbf{v}|^2 + |\mathbf{b}|^2\rangle/2$, the cross-helicity $H_c = \langle\mathbf{v}\cdot\mathbf{b}\rangle$, and the magnetic helicity $H_m = \langle\mathbf{a}\cdot\mathbf{b}\rangle$ are 3D ideal ($\nu = \eta = 0$) invariants. Dimensionless helicities are $\sigma_c = 2H_c/E$ and $\sigma_m = (E_L - E_R)/E_b$, where E_L and E_R are the energy in left- and right-handed magnetic polarizations, respectively.

Simulations.—We examine simulations (see Table I) of the MHD equations in a spatially periodic domain of side 2π, using a second order Runge-Kutta method, and either 2/3-rule dealiased [8], or non-dealiased pseudospectral methods. All runs freely decay in time, with no external forcing. The type labeled RAN are 128^3 incompressible runs, with random broadband initial conditions. Four cases have varying initial σ_m and σ_c, spanning a range of possibilities starting from a fully random state.

We employ other initial conditions with controlled helicities and more ordered fields. Orszag-Tang (OT) runs are a generalization of the 2D OT vortex [9], a standard large-scale initial condition for MHD turbulence. In our OT case,

TABLE I. Parameters for runs RAN, OT, and ABC (see text): N is the resolution, ν and η the viscosity and magnetic diffusivity, σ_c and σ_m the normalized cross and magnetic helicities.

Run	N^3 or N^2	$\nu = \eta$	σ_c	σ_m
RAN1	128^3	2.5×10^{-3}	0	0
RAN2	128^3	2.5×10^{-3}	0.5	0
RAN3	128^3	2.5×10^{-3}	0	0.5
RAN4	128^3	2.5×10^{-3}	0.5	0.5
OT1	128^3	5×10^{-3}	0.4	0
OT2	256^3	1.5×10^{-3}	0.4	0
OT3	512^3	7.5×10^{-4}	0.4	0
ABC1	128^3	3×10^{-3}	0	0.5
ABC2	256^3	1.25×10^{-3}	0	0.5
ABC3	512^3	6×10^{-4}	0	0.5
ABC4	1536^3	2×10^{-4}	0	0.5
2D	1024^2	2.5×10^{-4}	0	0

initially energies $E_v = E_b = 2$. The set of runs labeled ABC consists of a parametrized large-scale helical flow, an uncorrelated and helical large-scale magnetic field, and added noise with energy spectra $\sim k^{-3} \exp[-2(k/k_0)]^2$ at $t = 0$, with $k_0 = N/6$ [10]. These runs have $E_v = E_b = 0.5$, $\sigma_c \approx 1 \times 10^{-4}$, and $\sigma_m \approx 0.5$. Finally we analyze a small region near a current sheet in a very high-Reynilds-number ABC run.

Probability density functions (PDFs).—Our main diagnostics are PDFs of the local cosine of the angle θ between $\mathbf{v}$ and $\mathbf{b}$

$$\cos\theta = \cos\angle(\mathbf{v}, \mathbf{b}) = \frac{\mathbf{v} \cdot \mathbf{b}}{|\mathbf{v}||\mathbf{b}|}, \tag{3}$$

which are computed for each run. The PDFs for RAN2, shown in Fig. 1, at times $t = 0$, 0.5, 1.0, and 2.0, are highly peaked near $\cos\theta \approx 1$, much more so than would be needed to account for the cross-helicity (initially $\sigma_c \approx 0.5$, decaying to $\sigma_c = 0.24$ at $t = 2.0$). The more peaked curves are for the progressively later times. For RAN1, having no helicities (see Fig. 2), the PDFs are suppressed near $\cos\theta \approx 0$ and strongly peaked near $\cos\theta \approx \pm 1$. This indicates an enhanced probability of aligned or antialigned $\mathbf{v}$ and $\mathbf{b}$. This enhanced directional alignment occurs quickly and even when the global cross-helicity is ≈ 0; therefore, this process is distinct from long term or steady alignment discussed previously [4–6].

Results of RAN3 and RAN4, with $\sigma_m \approx 0.5$ (not shown) are almost indistinguishable from the corresponding case with $\sigma_m \approx 0$. The PDFs in the OT runs (also not shown) are asymmetric and strongly peaked at $\cos\theta \approx 1$, as in the RAN2 and RAN4 cases. For the ABC runs, with initial $\sigma_c = 0$, the PDFs peak at $\cos\theta \approx \pm 1$ after less than half a turnover time, following the pattern of the RAN runs. Figure 3 shows the PDFs from the ABC runs at the peak of dissipation ($t \approx 4$) for different Reynolds numbers. This local alignment process is fast in all cases, with substantial and apparently nearly saturated alignment occurring in less than one large-scale turnover time. No clear depen-

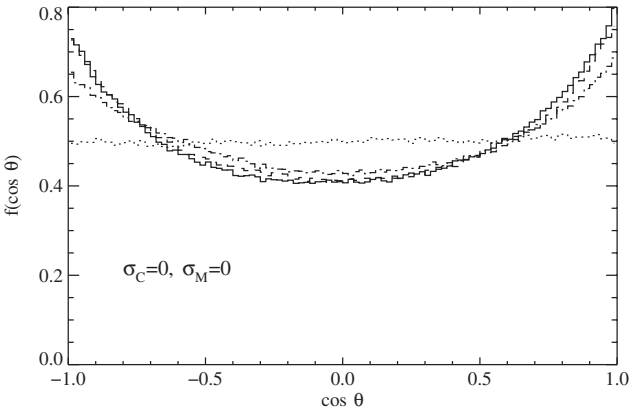

FIG. 2. PDFs of $\cos\theta$ at times $t = 0$ (flat, dotted line), 0.5 (dash-dotted line), 1.0 (dashed line), 2 (solid line) for 3D run RAN1, $\sigma_c \approx 0$, $\sigma_m \approx 0$.

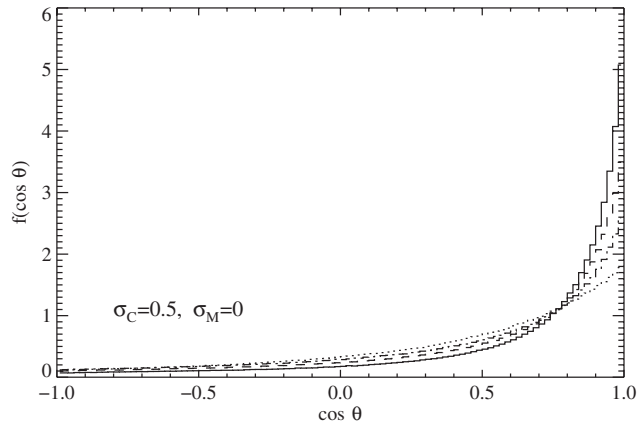

FIG. 1. PDFs of $\cos\theta$ for initial normalized cross-helicity $\sigma_c = 0.5$ for run RAN2. Global normalized cross-helicity is 0.24 at $t = 2$. Different lines are for different times (see text).

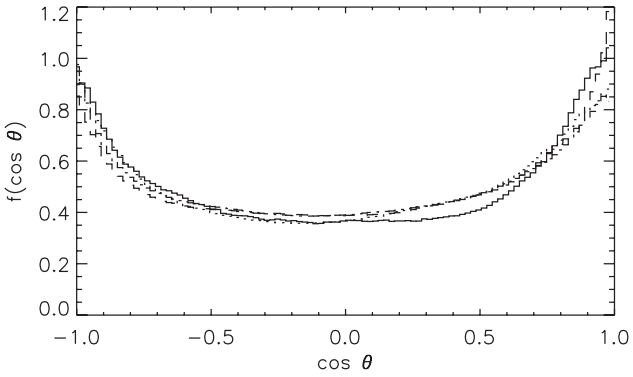

FIG. 3. PDFs of $\cos\theta$: runs ABC1 (solid line), ABC2 (dotted line), ABC3 (dashed line), ABC4 (dash-dotted line), at the peak of dissipation.

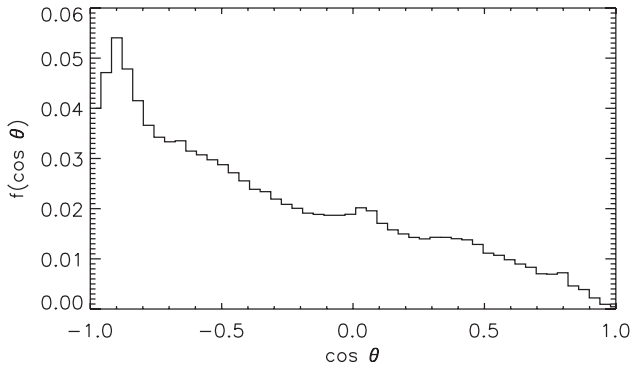

FIG. 4. PDF of cosθ near a current sheet (subvolume of 150^3 grid points) within 1536^3 run ABC4.

dence on Reynolds numbers is seen when comparing cases ABC1–4.

When PDFs of cosθ are computed in the vicinity of strong shear in the magnetic field (run ABC4), an only slightly different result is obtained (Fig. 4). Inside the associated current sheet, $\mathbf{v}$ and $\mathbf{b}$ are strongly antialigned (producing the peak near -1), and the PDF is linear. When larger subvolumes near the current sheet are considered, or at later times when more current sheets with different alignments are included in the subvolume, the PDF converges towards the form seen in Fig. 3.

Physics of alignment.—Why does local alignment take place in these simulations? And why is it so fast? Manipulating Eqs. (1) and (2) in the ideal case ($\nu = \eta = 0$), one finds the equation for evolution of the local cross-helicity:

$$\frac{\partial(\mathbf{v}\cdot\mathbf{b})}{\partial t} + \mathbf{v}\cdot\boldsymbol{\nabla}(\mathbf{v}\cdot\mathbf{b}) = \mathbf{b}\cdot\boldsymbol{\nabla}\frac{\mathbf{v}^2}{2} - \mathbf{b}\cdot\boldsymbol{\nabla}\mathcal{P}. \quad (4)$$

In the ideal, incompressible case, this equation embodies all effects that cause local change of $\mathbf{v}\cdot\mathbf{b}$. The equation for the evolution of cosθ contains additional terms associated with the rates of change of $|\mathbf{v}|$ and $|\mathbf{b}|$. Equation (4) is simple and revealing. The terms on the left are the convective derivative. The terms on the right are divergences: using that $\boldsymbol{\nabla}\cdot\mathbf{b} = 0$, and when integrated over volume with the proper boundary conditions (e.g., periodic boundaries), they vanish. This expresses the fact that the global cross-helicity is an ideal invariant.

However, kinetic energy and pressure gradients affect *local* alignment. The first term on the right of Eq. (4) shows that kinetic energy gradients (e.g., shear) changes alignment or $\mathbf{v}$ and $\mathbf{b}$ when $\boldsymbol{\nabla}|\mathbf{v}|^2$ is parallel to $\mathbf{b}$. Indeed, a magnetic field line (which acts as a material line by Alfvén's theorem) is distorted by shear and tends to align with the local $\mathbf{v}$. For a planar shear, this is similar to what is called field line stretching. From the second term on the right, $\boldsymbol{\nabla}\mathcal{P}$ parallel to $\mathbf{b}$ also changes the alignment. When the $\mathbf{v}$ is directed from a region of higher $\mathcal{P}$ towards lower $\mathcal{P}$, and $\boldsymbol{\nabla}\mathcal{P}$ has a projection onto $\mathbf{b}$, the local alignment of $\mathbf{v}$ and $\mathbf{b}$ increases. A direct numerical study (not shown) of the right-hand side of Eq. (4) using Table I simulation data confirms that these terms drive a tendency towards local alignment of $\mathbf{v}$ and $\mathbf{b}$. We can estimate the time for the local alignment to take place as $\sim b_l/l$, where b_l is the magnetic fluctuation amplitude at scale l. Since $b_l \sim v_l$ (the velocity amplitude at scale l), this time is proportional to the eddy turnover time.

Since Eq. (2) is formally equivalent to the hydrodynamic vorticity equation, analogous reasoning implies that the hydrodynamic velocity $\mathbf{v}$ and vorticity $\boldsymbol{\omega} = \boldsymbol{\nabla}\times\mathbf{v}$ tend to align locally. This is found numerically [7] in regions of low dissipation. Replacing $\mathbf{b}$ by $\boldsymbol{\omega}$ in Eq. (4), we see that alignment occurs when $\boldsymbol{\omega}$ is parallel to kinetic energy and pressure gradients.

Solar wind observations.—Using samples of spacecraft data we computed distributions of the alignment angle for two interplanetary data sets—the Omni data set at 1 A.U. near Earth orbit in the ecliptic plane, and a sample of Ulysses data from high heliographic latitude. Figure (5) shows the results of these analyses. The low latitude OMNI analysis is divided into intervals in which the large-scale interplanetary magnetic field is directed either away from or towards the sun. The sign of the average cross-helicity in the higher latitude Ulysses sample is associated with outward propagation. In each of these cases, the PDFs of the local alignment are consistent with the net cross-helicity in each sample.

Discussion and conclusions.— The characteristic PDFs of cosθ described above cannot be explained as a superposition of uncorrelated Gaussian distributions for the velocity and magnetic field components, although the PDFs of the velocity and magnetic field themselves are Gaussian (but clearly correlated). PDFs computed from random broadband uncorrelated Gaussian-component ve-

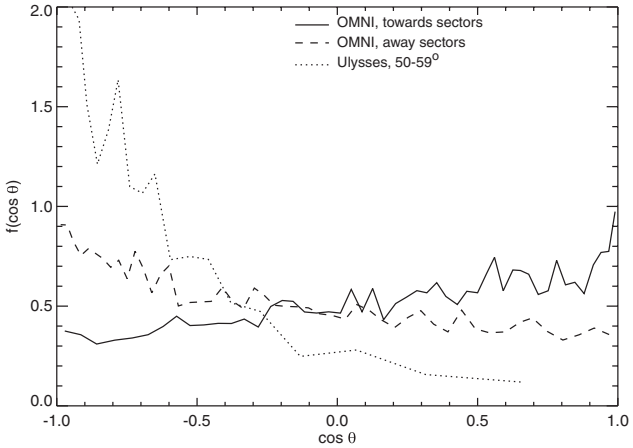

FIG. 5. PDF of cos(θ) from 30 years of Omni data (ISEE, IMP, and other satellite data), and from Ulysses spacecraft data between 50° and 59° heliospheric north latitude during a polar pass in solar minimum conditions.

FIG. 6. Two-dimensional incompressible MHD simulation, showing areas where $\cos\theta < -0.7$ (black), $|\cos\theta| < 0.7$ (gray), and $\cos\theta > 0.7$ (white). Areas with highly aligned or antialigned velocity and magnetic field dominate the picture.

locity and magnetic fields have a flat $f(\cos\theta)$ distribution. For the coherent ABC flows, $\cos\theta$ peaks at 0 initially, while for the nonhelical RAN1 and RAN3 flows the distribution is initially flat. All cases evolve towards the characteristic shape that is highly peaked at $|\cos\theta| = 1$. In contrast, prior studies have shown that the distribution of the induced electric field, $-\mathbf{v} \times \mathbf{b}$, is accurately computed from Gaussian statistics, for both high and low cross-helicity, in simulations and in solar wind data [11]. What apparently accounts for the difference is that the induced EMF does not correspond to a conserved quantity, while the alignment angle is closely associated with the ideally conserved cross-helicity. The EMF can be accounted for using Gaussian statistics, but alignment, even of Gaussian fields, is a dynamical quantity constrained by the local transport and conservation, as implied by Eq. (4).

Note that Alfvén vortices [12], which are coherent structures predicted for reduced MHD, have been recently observed in space plasmas [13]; the generalized Alfvén condition found in these vortices corresponds to a local directional alignment. Evidently this type of robust alignment process may be influential in a variety of space and astrophysical plasmas as well as in neutral fluids.

We conclude that directional alignment is a rapid and robust process in turbulence. The magnetic and velocity fields respond to the local values of the shear and pressure gradients, essentially independently of the conditions at remote locations, leading to local alignment or antialignment. Figure 6 illustrates this localization or patchiness of the directional alignment, using a 2D MHD simulation (see also [14]). Since the alignment appears to be a universal and rapid process, it would not be surprising if coherent small scale structures in MHD turbulence are associated with it. Indeed, Fig. 4 is an example where coherent current sheets are observed to have maximum alignment between the velocity and the magnetic fields [10]; similarly the local $\mathbf{v}$-$\boldsymbol{\omega}$ alignment may explain the slow return to full isotropy in fluid turbulence.

Research supported by NSF ATM-0539995, NASA NNG06GD47G, NNX08AI47G (Heliophysics Theory Program), and NCAR. P. D. M. and P. D. are members of the Carrera del Investigador Científico of CONICET.

[1] L. Woltjer, Proc. Natl. Acad. Sci. U.S.A. **44**, 833 (1958).
[2] J. W. Belcher and L. Davis, J. Geophys. Res. **76**, 3534 (1971).
[3] B. Bavassano *et al.*, Sol. Phys. **78**, 373 (1982); D. A. Roberts *et al.*, J. Geophys. Res. **92**, 12023 (1987).
[4] M. Dobrowolny, A. Mangeney, and P. Veltri, Phys. Rev. Lett. **45**, 144 (1980); A. Pouquet, U. Frisch, and M. Meneguzzi, Phys. Rev. A **33**, 4266 (1986); R. Grappin *et al.*, Astron. Astrophys. **105**, 6 (1982); W. H. Matthaeus, M. L. Goldstein, and D. Montgomery, Phys. Rev. Lett. **51**, 1484 (1983).
[5] A. C. Ting, W. H. Matthaeus, and D. Montgomery, Phys. Fluids **29**, 3261 (1986); T. Stribling and W. H. Matthaeus, Phys. Fluids B **3**, 1848 (1991).
[6] J. Mason *et al.*, Phys. Rev. Lett. **97**, 255002 (2006); S. Boldyrev, Phys. Rev. Lett. **96**, 115002 (2006).
[7] R. Pelz *et al.*, Phys. Rev. Lett. **54**, 2505 (1985); H. K. Moffatt, J. Fluid Mech. **159**, 359 (1985); A. Tsinober and E. Levich, Phys. Lett. **99A**, 321 (1983); E. Levich, Phys. Rep. **151**, 129 (1987); M. Farge, G. Pellegrino, and K. Schneider, Phys. Rev. Lett. **87**, 054501 (2001).
[8] S. A. Orszag and G. S. Patterson, Phys. Rev. Lett. **28**, 76 (1972).
[9] S. A. Orszag and C.-M Tang, J. Fluid Mech. **90**, 129 (1979).
[10] P. Mininni, A. Pouquet, and D. Montgomery, Phys. Rev. Lett. **97**, 244503 (2006); P. Mininni and A. Pouquet, arXiv:abs/0707.3620v1.
[11] B. Breech *et al.*, J. Geophys. Res. **108**, 1153 (2003).
[12] V. I. Petviashvili and O. A. Pokhotelov, in *Solitary Waves in Plasmas and in the Atmosphere* (Gordon & Breach, New York, 1992).
[13] D. Sundkvist *et al.*, Nature (London) **436**, 825 (2005); O. Alexandrova *et al.*, J. Geophys. Res. **111**, A12208 (2006).
[14] M. Meneguzzi *et al.*, J. Comput. Phys. **123**, 32 (1996).